Transition to the open state of the TolC periplasmic tunnel entrance

Christian Andersen, Eva Koronakis, Evert Bokma, Jeyanthy Eswaran, Daniel Humphreys, Colin Hughes, and Vassilis Koronakis*

Department of Pathology, Cambridge University, Tennis Court Road, Cambridge CB2 1QP, United Kingdom

Edited by Richard Henderson, Medical Research Council, Cambridge, United Kingdom, and approved June 19, 2002 (received for review January 23, 2002)

The TolC channel-tunnel spans the bacterial outer membrane and periplasm, providing a large exit duct for protein export and multidrug efflux when recruited by substrate-engaged inner membrane complexes. The sole constriction in the single pore of the homotrimeric TolC is the periplasmic tunnel entrance, which in its resting configuration is closed by dense packing of the 12 tunnel-forming α-helices. Recruitment of TolC must trigger opening for substrate transit to occur, but the mechanism underlying transition from the closed to the open state is not known. The high resolution structure of TolC indicates that the tunnel helices are constrained at the entrance by a circular network of intra- and intermonomer hydrogen bonds and salt bridges. To assess how opening is achieved, we disrupted these connections and monitored changes in the aperture size by measuring the single channel conductance of TolC derivatives in black lipid bilayers. Elimination of individual connections caused incremental weakening of the circular network, accompanied by gradual relaxation from the closed state and increased flexibility of the entrance. Simultaneous abolition of the key links caused a substantial increase in conductance, generating an aperture that corresponds to the modeled open state, with the capacity to allow access and passage of diverse substrates. The results support a model in which transition to the open state of TolC is achieved by an iris-like realignment of the tunnel entrance helices.

The TolC family of envelope proteins is ubiquitous throughout Gram-negative bacteria and is central to type I secretion of toxins and proteases (1–4), and to the efflux of small noxious compounds, notably detergents and a wide range of antibacterial drugs (5, 6). It is therefore important to bacterial survival, especially in infections during which it mediates multidrug resistance and contributes to virulence (7, 8). At 2.1 Å resolution the TolC homotrimer is seen as a 140 Å long hollow conduit (Fig. 1*A*), comprising a 100 Å long α-helical barrel, the tunnel domain, projecting across the inter-membrane periplasmic space and anchored in the outer membrane by a contiguous 40 Å long β-barrel domain (9, 10). The average accessible interior diameter of the single central pore of TolC is 19.8 Å (30 Å measured from backbone to backbone) throughout the outer membrane channel and most of the tunnel. The channel exit is constitutively open.

The α-barrel is a novel structure in which 12 α-helices (four from each monomer) pack in an antiparallel arrangement to form a hollow cylinder. The structural principles and forces that constrain the α-helices in the α-barrel domain have been described in detail (9, 11). Throughout the α-barrel domain, the helices follow a left-handed superhelical twist but tend to be under-wound in the top one-half of the structure compared to helices in a conventional two-stranded coiled coil. This enables the helices to lie on the surface of a cylinder. The 12 helices pack laterally side-by-side and therefore form two separate interfaces, which are stabilized by an intermeshing of side-chains that is commonly referred to as ''knobs-into-holes'' packing.

In the lower half of the α-barrel, neighboring helices form six pairs of regular two-stranded coiled coils. At the periplasmic end of the tunnel, three of them (one from each monomer) fold inwards to constrict the periplasmic entrance to a resting closed state, determining an effective diameter of ≈3.9 Å (ref. 9; Fig. 1*B*). This small opening is consistent with electrophysiological characterization of TolC assembled in planar lipid bilayers, which has shown that TolC generates only a small conductance of about 80 pS in 1 M KCl (12, 13). In addition to their interfaces, the entrance coiled-coils also form contacts with each other. The closed conformation is very stable, which is reflected in the low thermal factor of this domain apparent in the crystallographic data and indicates restricted flexibility (9). The average B value (thermal factor) for the α-barrel up to 30 Å from the periplasmic TolC entrance is 33.8, compared to an average of 49.88 for the entire TolC structure.

When TolC is recruited by substrate-laden complexes in the inner membrane (3, 10, 14) during protein export and drug efflux, the closed periplasmic entrance must be opened for substrates to gain access to the exit duct. An allosteric mechanism for tunnel opening has been proposed, based on the observation that the three inner coiled coils (comprising helices H7 and H8), differ from the outer coiled coils (H3/H4) only by small changes in superhelical twist (9). In the proposed mechanism, it is envisaged that transition to the open state could be achieved by the inner coils undergoing a movement to realign with the outer coils, thereby enlarging the aperture diameter (Fig. 1*C*).

The high resolution structure of TolC shows a circular network of inter- and intramolecular connections near the tunnel entrance that maintains the coiled coil packing and so constrains the three inner coils in the closed conformation (Fig. 1 *B* and *D*). To appraise the proposed opening mechanism, we have disrupted the hydrogen bonds and salt bridges that appear central to the arrangement of the α-helices. As the periplasmic entrance is the sole constriction of the 140 Å long pore (9, 10), changes in the diameter of the aperture could be monitored by comparing the conductance of TolC wild-type (WT) and variants in black lipid bilayers.

Materials and Methods

Creation of TolC Mutant Variants. Mutations were introduced into *tolC* by using the QuikChange site-directed mutagenesis method (Stratagene). A template plasmid was created by subcloning 1.8-kbp (*Pst*I–*Bam*HI) sequence of plasmid pT7TolC (9) into *Pst*I–*Bam*HI treated vector pUC19 (15). The double-stranded plasmid was denatured and for each substitution two mutagenic primers of complementary sequence were annealed. Both DNA strands were extended and amplified with *Pfu* Turbo polymerase in 12–18 cycles of PCR. The parental WT template strands were removed by digesting with *Dpn*I endonuclease. Mutations were confirmed by nucleotide sequence analyses after transformation of *Escherichia coli* cells. Double-stranded DNA fragments encompassing the mutagenized sites were cloned back into the WT plasmid pT7TolC. The 5′–3′-sequences of the forward oligonu-

This paper was submitted directly (Track II) to the PNAS office.

Abbreviation: WT, wild type.

*To whom reprint requests should be addressed. E-mail: vk103@mole.bio.cam.ac.uk.

BIOCHEMISTRY

cleotide primers are listed below, the reverse primers are complementary to these.

$T^{152}V$: GTGGGCCTGGTAGCGATCGTCGACGTGCAGAACGCC; $D^{153}A$: GCCTGGTAGCGATCACGGCCGTGCAGAACGCCCG; $E^{359}A$: GCTCATTAGACGCGATGGCAGCCGGCTACTCGGTCGGTAC; $Y^{362}F$: GCGATGGAAGCGGGCTTCTCGGTCGGTACCCGTACCATTGTT; $R^{367}S$: GGCTACTCGGTCGGTACGAGTACTATTGTTGATGTGTTG; $T^{152}VD^{153}A$: GGCCTGGTAGCGATCGTCGCCGTGCAGAACGCCCGC; $Y^{362}FR^{367}S$: GCGATGGAAGCGGGCTTCTCGGTCGGTACGAGTACTATTGTTGATG.

Variants $T^{152}VD^{153}AE^{359}A$ and $T^{152}VD^{153}AR^{367}S$ were created by ligating DNA fragments containing single substitutions $R^{367}S$ or $E^{359}A$ into the $T^{152}VD^{153}A$ plasmid.

TolC-Dependent Protein Export and Drug Resistance. Protein export was assayed in *E. coli* BL923 transformants expressing WT or variant TolC and also the export proteins HlyB and HlyD from the hemolysin operon of plasmid pEK50 (16). Cultures were grown in 2xTY broth (1.6% tryptone/1% yeast extract/0.5% sodium chloride) to early exponential phase ($A_{600} = 0.4$). Exported HlyA was precipitated from the cell-free supernatant and assayed by SDS/10% PAGE and immunoblotting with anti-HlyA sera. Drug resistance of the same transformants was assessed by the ability to grow in LB broth inoculated 1:1,000 with overnight cultures and/or by growth up to inhibitor discs on LB agar plates.

Overexpression and Purification of TolC Proteins. TolC proteins were purified from 100 ml of isopropyl β-D-thiogalactoside-induced cultures of the TolC-negative strain *E. coli* BL923(DE3) (3) carrying the recombinant plasmid pT7TolC or mutated derivatives. Cells were broken in a French Press, and TolC proteins were purified from membranes as described (9, 17).

Electrophysiological Analyses in Lipid Bilayers. Black lipid membranes were formed as described (18). Instrumentation comprised a Teflon chamber with two aqueous compartments connected by a circular hole of 0.5-mm diameter. Membranes were formed by painting onto the hole a 1% solution of diphytanoyl phosphatidycholine (Avanti Polar Lipids) in *n*-decane. Experiments were performed in 1 M KCl (Aldrich, 99.999% pure) at room temperature. The TolC proteins were diluted and added to one side of the membrane, the cis side. The membrane current was measured with a pair of calomel electrodes switched in series with a voltage source and an electrometer (Keithley 6517A). The membrane potential is always given with respect to the cis side. For single channel recordings, the electrometer was replaced by a current-amplifier (Keithley 428). The amplified and filtered signal (filter rise time 30 ms) was monitored with a strip chart recorder and sampled (50 s^{-1}) by a personal computer connected to the output signal by an AD-converting card (Keithley DAS-1601).

Results

A Network of Interhelical Links Central to the Entrance Closed State. The resting closed state and modeled open state of the periplasmic entrance have been described following elucidation of the TolC high resolution structure (9) and are presented in Fig. 1 *B* and *C*. Comparison of the two states identifies three key links that establish a circular network constraining the six helical pairs in the closed state (Fig. 1*D*). Links I and II connect each inner coiled coil to the outer coil of the same monomer by hydrogen bonds between Asp^{153}–Tyr^{362} and Gln^{136}–Glu^{359}, respectively. Link III connects Arg^{367} of each inner coiled coil to the outer coil of the adjacent monomer, by a salt bridge to Asp^{153} and a hydrogen bond to Thr^{152} (Fig. 1*D*). The analysis suggests that for the inner coiled coils to move outwards and enlarge the entrance diameter, these links must be disrupted.

Interrupting the Interhelical Links Weakens the Entrance Closed State. To prevent formation of the salt bridge and hydrogen bonds, *in vitro* mutagenesis was used to introduce single substitutions of critical residues (Fig. 1*E*). These residues do not directly influence the entrance diameter as they are not located at the narrowest point of the constriction [this is lined by a ring of six aspartate residues (17) located on the inner coil one and two helix turns above Arg^{367}], and the substitutions did not introduce opposite charges or greater bulk. The intramonomer hydrogen bond Asp^{153}–Tyr^{362} (link I) was disrupted by substituting Tyr^{362} by phenylalanine (mutant $TolC^{Y362F}$ abbreviated as $TolC^{YF}$) or by substituting Asp^{153} by alanine ($TolC^{DA}$). The intramonomer hydrogen bond Gln^{136}–Glu^{359} (link II) was prevented by exchange of Glu^{359} by alanine ($TolC^{EA}$). The intermonomer salt bridge Arg^{367}–Asp^{153} (link III) was targeted by replacing Arg^{367} by serine ($TolC^{RS}$), or by substituting Asp^{153} by alanine (again $TolC^{DA}$) (Fig. 1*E*). The additional hydrogen bond formed between Arg^{367} and Thr^{152} was abolished in $TolC^{RS}$ and also by substitution of Thr^{152} by valine ($TolC^{TV}$).

That the TolC variants retained *in vivo* function was confirmed by assaying TolC-dependent export of the 110-kDa protein substrate hemolysin (HlyA). Cell-free culture supernatants were collected from *E. coli* BL923 transformants expressing WT or mutant TolC and the inner membrane proteins HlyB and HlyD, which recruit TolC to the export apparatus (3). Immunoblotting of extracellular HlyA (Fig. 2) showed that the mutant TolC proteins substituted fully for the WT TolC. In parallel, growth of the same transformants was not inhibited by 0.05% sodium deoxycholate or 50 μg/ml novobiocin, both substrates of the TolC multidrug resistance pump (19), in contrast to the *tolC*-negative mutant *E. coli* BL923 (3), which did not grow in the presence of deoxycholate and was inhibited by 0.4 μg/ml novobiocin.

All variant TolC proteins could be isolated as trimers from *E. coli* membrane fractions. In parallel with $TolC^{WT}$, the five mutant proteins were purified to homogeneity and reconstituted in planar lipid bilayers. TolC inserts into bilayers in one orientation, β-barrel domain first as would occur in the cell (12). Throughout the current study, TolC proteins were added to one side of the membrane only, so the tunnel entrance always faces the side (the cis or periplasmic side, Fig. 1*A*) from which the protein is added. TolC characteristics could therefore be studied in relation to membrane potential, positive or negative, quoted with respect to this cis side.

Each of the five mutant proteins, $TolC^{TV}$, $TolC^{EA}$, $TolC^{YF}$, $TolC^{DA}$, and $TolC^{RS}$, formed stable, functional channels. At +/−80 mV the conductances of $TolC^{TV}$ and $TolC^{EA}$ were indistinguishable from $TolC^{WT}$, but $TolC^{YF}$, $TolC^{DA}$, and $TolC^{RS}$ conductances were higher (Fig. 3 *A* and *B*), indicating increases in the size of the entrance diameter. $TolC^{DA}$ was characterized by regular, reversible switches into a smaller conductance state (65% that of its conductance at +80 mV). Defined substates are also seen with TolC WT (12), but their significance is not known. $TolC^{RS}$ was characteristically noisy (Fig. 3*A*), and at negative potentials greater than −60 mV, it switched infrequently into various states with a conductance 40–115% that of the main state (not shown).

Weakening the Closed State Increases Flexibility of the Entrance Configuration. Single channel conductances of $TolC^{WT}$ and the five variants were measured over a range of potentials and the main conductances (maximum observed values at each voltage) were plotted (Fig. 3*B*). Like the WT, the conductance of all of the variants was roughly constant over the range of positive potentials (reflecting the "resting state" conductance) but in-

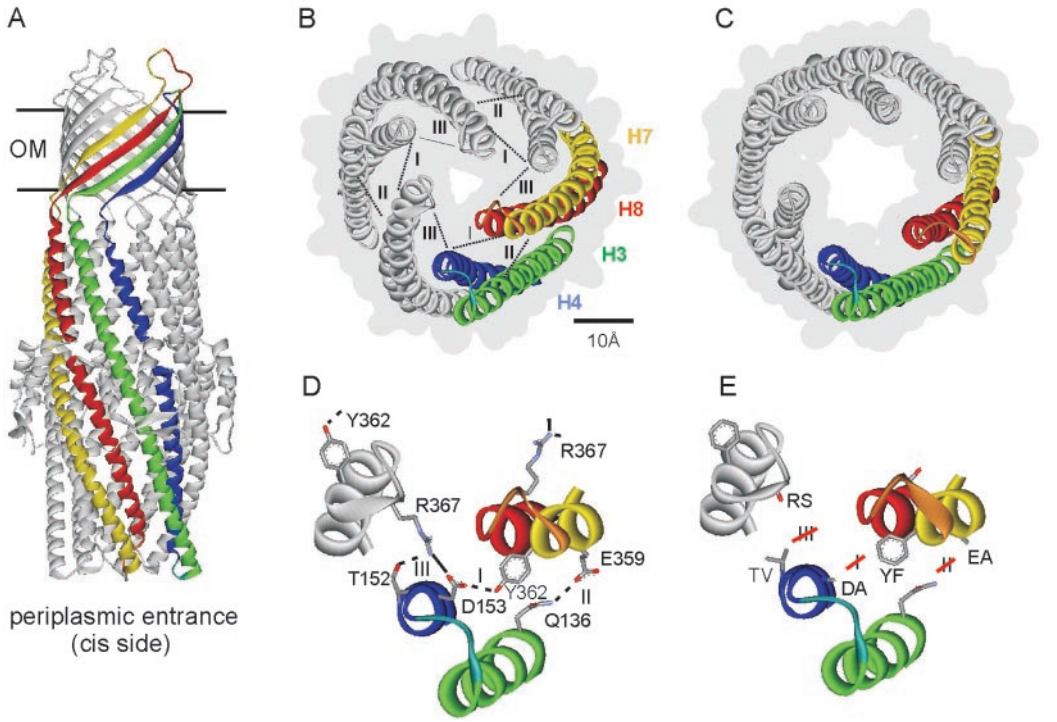

Fig. 1. The structure of TolC and its periplasmic entrance. (*A*) The TolC structure (9) is 140 Å in length. The 40 Å long β-barrel domain spanning the outer membrane (OM) is assembled from 12 β-sheets (four per monomer) and is constitutively open. The 100 Å long α-helical domain is formed by 12 α-helices and projects across the periplasmic space. The entrance is located at the bottom of this domain as indicated. One monomer is highlighted in the same color scheme as in *B*. (*B*) The closed state of the entrance seen from the periplasmic side. Helices of one of the three monomers are colored green (H3, outer coiled coil), blue (H4, outer), yellow (H7, inner coiled coil), and red (H8, inner). The numbering of the helices is taken from the high resolution structure (9). The connecting turns between H3/H4 and between H7/H8 are shown respectively in light blue and orange. Intramonomer (I and II) and intermonomer connections (III) are shown as dotted lines. The gray background outlines the surface representation, showing the small periplasmic entrance. (*C*) The modeled open state of the entrance (9), derived by realigning the inner coiled coils (H7/H8) to the same configuration as the outer coiled coils (H3/H4). (*D*) Magnification of the circular network at the tunnel entrance, showing the residues central to the intramonomer (I and II) and intermonomer (III) links. The salt bridge is shown in full, the hydrogen bonds are indicated by broken lines. (*E*) Substitutions made to disrupt the hydrogen bonds and salt bridge shown in *D*. Depictions were generated by using WEBLAB VIEWERLITE (Molecular Simulations, Cambridge, U.K.).

creased steadily with increasing negative potential. The conductances of $TolC^{TV}$ and $TolC^{EA}$ were identical to $TolC^{WT}$, at positive potentials remaining close to 80 pS and increasing to 92 pS at −100 mV. The corresponding conductances of $TolC^{YF}$ were 120/150 pS, $TolC^{DA}$ 180/247 pS, and $TolC^{RS}$ 205/371 pS, showing not only the increases in resting conductance, but also a concomitant amplification of the maximum values at negative potentials. The ratio between the conductances at +80 mV (resting) and −100 mV (amplified) was 1.15 for $TolC^{WT}$, $TolC^{TV}$, and $TolC^{EA}$, but it was 1.25 for $TolC^{YF}$, 1.37 for $TolC^{DA}$, and 1.81 for $TolC^{RS}$. The amplification suggests that the aperture enlarges further at higher negative potential, as pressure is exerted by high cation flux through the tunnel toward the entrance. This reflects increasing flexibility of the entrance helices in the TolC variants.

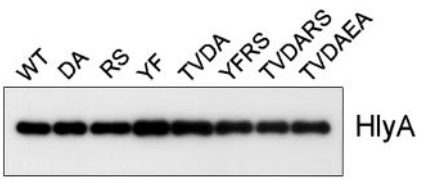

Fig. 2. TolC-dependent protein export from *E. coli*. Cell-free supernatants (100 μl) of exponentially growing cultures of *E. coli* BL923 expressing either WT or mutant TolC protein were subjected to SDS/PAGE and blotted with anti-HlyA antiserum.

Simultaneous Disruption of the Key Links Opens the Entrance. Substitutions $R^{367}S$ and $D^{153}A$ had the largest effects. $R^{367}S$ prevents both the salt bridge and hydrogen bond components of intermonomer link III, whereas $D^{153}A$ precludes the same salt bridge, and also the intramonomer hydrogen bond (link I). By combining single substitutions based on R^{367} and D^{153}, further variants were constructed in which key connections were disrupted simultaneously. Like the single mutants, these TolC variants appeared fully active in protein export (Fig. 2) and also had the same levels of novobiocin and deoxycholate resistance (not shown). The purified proteins formed stable pores in artificial bilayers (Fig. 4*A*).

$TolC^{TVDA}$ conductance was very similar to $TolC^{DA}$ over the range −100 mV to +100 mV (Fig. 4*B*), with a constant 180 pS at positive potential, increasing to 210 pS at −100 mV. Single channel recordings showed that like $TolC^{DA}$, $TolC^{TVDA}$ switches regularly into a lower conductance state, but in $TolC^{TVDA}$ this lower state is closer to its main conductance state. The data indicate that although the TV substitution does influence the low conductance state, it causes little or no additional weakening of connection III. Adding the $E^{359}A$ substitution to $TolC^{TVDA}$ to create $TolC^{TVDAEA}$ confirmed the indication from analysis of $TolC^{EA}$, that disruption of the intramolecular hydrogen bond II located at the periphery of the tunnel has little or no effect on the opening. $TolC^{TVDAEA}$ channels behaved like $TolC^{TVDA}$ with conductance only marginally increased (Fig. 4*B*).

In $TolC^{TVDARS}$ the connections disrupted are the same as in $TolC^{TVDA}$, but in addition the positive charge of R^{367} is removed.

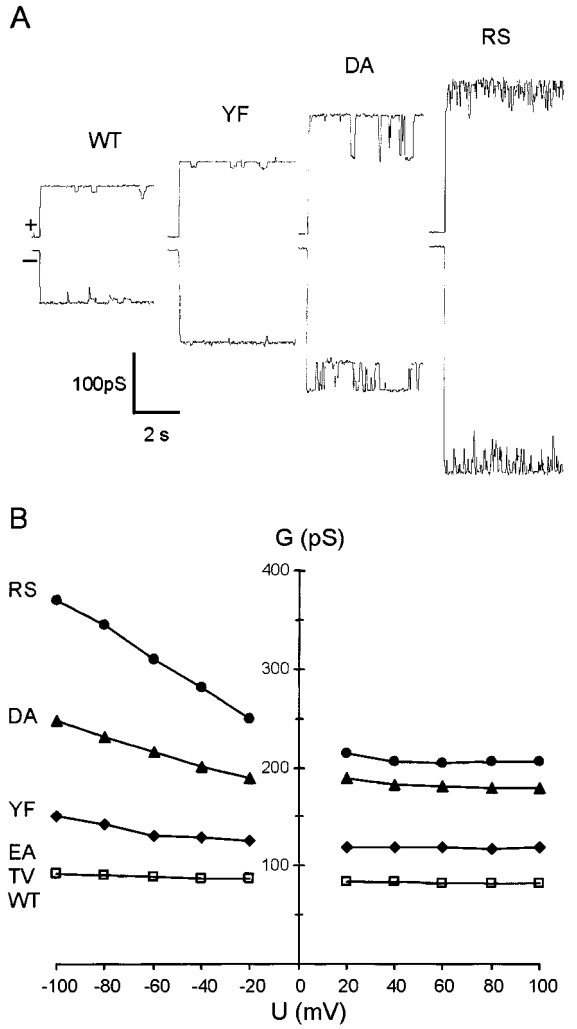

Fig. 3. Single channel conductance of TolC variants with single substitutions. (*A*) At +80 mV (upper trace) and −80 mV (lower trace). (*B*) Dependence on applied membrane potential. Each point represents the main (maximum) conductance achieved at the voltage. Proteins were added to the cis side of the membrane bathed in 1 M KCl, pH 7.5.

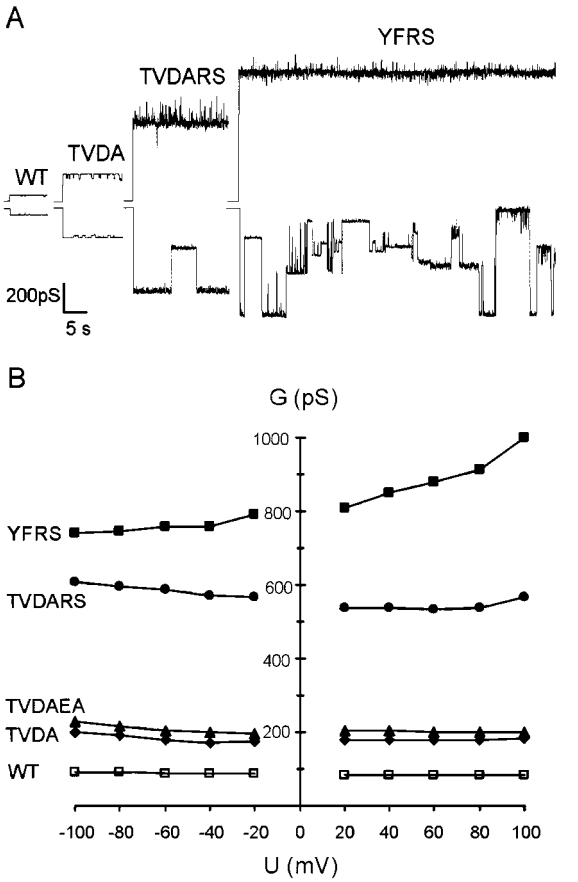

Fig. 4. Single channel conductance of TolC variants with multiple substitutions. (*A*) At +80 mV (upper trace) and −80 mV (lower trace). (*B*) Dependence of the main conductance on applied membrane potential. Conditions as in Fig. 3.

This had a dramatic effect, as TolC^{TVDARS} channels showed a minimum conductance above 500 pS, 6-fold higher than that of the WT and 3-fold higher than TolC^{TVDA}. Conductance was again roughly constant at positive potentials, although noisy with higher conductance spikes, and increased at higher negative potentials. Like TolC^{RS}, TolC^{TVDARS} switched reversibly into various substates at negative potentials higher than −60 mV (an example is shown in Fig. 4*A*). A still greater increase in conductance resulted from combination of $R^{367}S$ (precludes link III) and $Y^{362}F$ (prevents link I). TolC^{YFRS} had a single channel conductance between 800 pS and 1,000 pS. The influence of the membrane potential on conductance differed from the other mutants, increasing with rising positive potential (Fig. 4*B*). At positive potentials (and at negative potentials below −60 mV, not shown), the TolC^{YFRS} high conductance state was stable, but above −60 mV it became highly unstable, the lifetime of the open state was short and there were frequent switches into several apparently random conductance states, including complete closure (Fig. 4*A*). The electrophysiological behavior of TolC^{YFRS} indicates significant destabilization of the tunnel closed state.

Discussion

We set out to establish how the TolC periplasmic tunnel entrance is opened, a critical event in its function during protein export and multidrug efflux. To do this we disrupted the circular network of intra- and interprotomer connections that the structure indicates constrain the inner coiled coils of the tunnel entrance in their closed conformation (9). The mutant variants functioned comparably to the WT TolC *in vivo*, and purified mutant proteins assembled normally into planar lipid bilayers. Destabilization of the closed state and transition to the open configuration could therefore be monitored by measuring conductance.

The conductances of TolC^{EA} and TolC^{TV} were unchanged from TolC^{WT}, indicating little or no importance for the intramonomer link II, a hydrogen bond located at the periphery of the tunnel, or the hydrogen bond component of intermonomer connection III. The moderate 1.3-fold increase in the conductance of TolC^{YF} is compatible with disruption of intramonomer connection I, the hydrogen bond D^{153}-Y^{362}, allowing the inner coiled coil to move slightly outwards and enlarge the constriction diameter. More substantial increases in conductance, 2.2- and 2.5-fold, resulted from the substitutions of TolC^{DA} and TolC^{RS}, both of which targeted the R^{367}-D^{153} salt-bridge of intermonomer connection III. These results were consistent with partial release of the inner coiled coils from their constrained position causing incremental weakening of the network. The resulting enlargements of the resting aperture, seen as the generally stable conductances over the range of positive potentials, may be driven by release of tension inherent in the packing of the supertwisted

coils (11) and/or electrostatic repulsion exerted by the ring of six aspartate residues (D^{371} and D^{374}) lining the narrowest point of the constriction (17). The effect may also be influenced by changes in charge arising from replacement of D^{153} or R^{367} by uncharged residues.

The conductances were amplified with rising negative potential, possibly illustrating progressive opening of the entrance under the pressure of high cation flux through the tunnel. This is seen to a mild degree in $TolC^{WT}$ (12), $TolC^{TV}$, and $TolC^{EA}$ but was increasingly evident in the variants $TolC^{YF}$, $TolC^{DA}$, and $TolC^{RS}$, as maximum conductances were, respectively, 38%, 52%, and 95% higher than resting conductances (compared to 12% for $TolC^{WT}$). This voltage-linked amplification reflects increasing flexibility of the helices forming the entrance structure. No precedent has been described for this behavior, which is quite distinct from the voltage-dependent "gating" seen in porins and other channels.

The $TolC^{DA}$ and $TolC^{RS}$ behavior highlighted the importance of the intermonomer link III, and substitutions were combined with the aim of allowing further movement of the inner coiled coil. $TolC^{TVDA}$ had a resting conductance very similar to that of $TolC^{DA}$, about 2.2-fold that of the WT, indicating that loss of the R^{367}–T^{152} hydrogen bond component of link III had no additional impact on the opening. $TolC^{DA}$ and $TolC^{TVDA}$ shared a characteristic pattern of switching into conductance substates, indicating two possible entrance conformations, a main conductance state common to both variants and a lower state apparently determined by the TV substitution. In $TolC^{TVDA}$ both components of link III and also intramonomer link I (D^{153}–Y^{362}) are disrupted, so the inner coiled coil of each protomer is entirely free from its constraints. The same bonds were targeted in a different way when the $TolC^{RS}$ substitution was combined independently with TVDA and YF. $TolC^{YFRS}$ has lost links I and III, while adding the RS change to TVDA in $TolC^{TVDARS}$ did not disrupt any further connection. In both cases the effect on the conductance was synergistic, dictating a 6-fold ($TolC^{TVDARS}$) to 10-fold ($TolC^{YFRS}$) increase over WT.

That their conductances are higher than that of $TolC^{TVDA}$ can be explained by the character of the residues D^{153} and R^{367}. Substitution of R^{367} removes a positive charge and could result in increased electrostatic repulsion between the remaining negative residues, enhancing the aperture diameter when the constraining network is relaxed. Substituting R^{367} could also allow D^{153}, D^{371}, and D^{374}, each located at the extremity of its coiled coil (9), to be attracted "downwards" away from the bilayer, at positive potentials, depending on the (unknown) residual strength of the potential gradient at this point. This would increase the effective diameter of the aperture in the $TolC^{YFRS}$ and $TolC^{TVDARS}$ variants. In contrast, $TolC^{DA}$ and $TolC^{TVDA}$ have lost the negatively charged partner of R^{367} in the salt bridge. This leaves the about 3 Å long flexible side chain of the unpaired R^{367} to possibly form new links—e.g., a salt bridge to D^{371} (neutralizing its negative charge)—or even intrude into the constriction, in each case quenching increases in conductance.

In agreement with this analysis, the R^{367}S-based variants differed substantially in their dependence on membrane potential. $TolC^{YFRS}$ in particular showed strong amplification at positive potentials, reaching 1,000 pS. Again this could reflect the strong net negative charge at the entrance enhancing the opening at high positive potentials. This effect would be expected to hold the entrance in a stable open conformation, and this stability was clearly evident in the experiments performed at positive potentials. In contrast to this stable opening, at high negative potential the open configuration of $TolC^{YFRS}$ became very unstable, with frequent switches into several lower conductance states (Fig. 4*A*). It seems plausible that this reflects the unrestrained flexible inner helices intermittently collapsing into the tunnel lumen. This would support the notion that the open conformation has to be transiently stabilized *in vivo* to allow substrate passage.

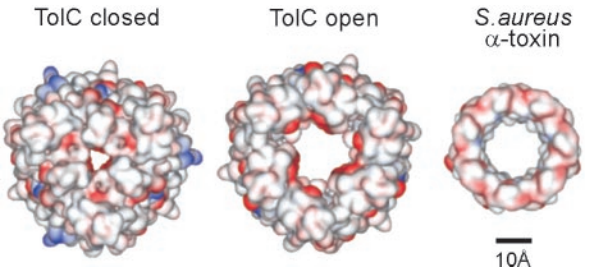

Fig. 5. Putative size of the opened entrance. Comparison of the modeled open state of the TolC entrance (*Center*) with the actual closed state (*Left*) (9) and the *Staphylococcus aureus* α-toxin membrane domain (*Right*) (22). The surface representations show electronegative and electropositive surfaces colored red and blue, respectively (generated by using WEBLAB VIEWERLITE, Molecular Simulations).

Because of the unique structure of TolC and the complex dependence of TolC conductance on parameters like membrane potential, electrolyte concentration, pH, and ion selectivity (12), it might be difficult to translate the conductances achieved into an accurate estimate of the aperture diameter in the open state. However, the conductances of $TolC^{YFRS}$ and $TolC^{TVDARS}$ are in the same range as that of the heptameric pore-forming α-hemolysin toxin of *Staphylococcus aureus* (Fig. 5), which has a membrane conductance of 1,000 pS in 1 M KCl (20, 21). The structure of the toxin pore is known. Formed by a membrane-spanning domain of 14 antiparallel β-strands, the pore has a diameter of 16 Å and the length of the entire structure is 100 Å (22, 23). Notwithstanding the cautions expressed above, extrapolating the change in conductance from the 80 pS ($TolC^{WT}$) closed state to 1,000 pS (amplified $TolC^{YFRS}$) as a function of the cross sectional area of the minimum circular aperture indicates a similar open state diameter. Such an aperture would allow exit of diverse substrates, even large partially unfolded proteins.

Our results show that the circular network of links near the entrance is important to maintaining the closed state of the TolC tunnel. They indicate that weakening these links, especially between the monomers, relaxes the helical arrangement, increasing the flexibility of the entrance and opening the constriction. *In vivo* this allosteric transition would be triggered when TolC is recruited by the large periplasmic domain of the inner membrane adaptor protein in response to substrate engagement at its cytosolic domain (3, 14). This interaction could, in an as yet undefined way, initiate destabilization of the TolC entrance network by disturbing one or more critical links, perhaps the intermonomer salt bridge D^{153}-R^{367}. The open state could then be stabilized or "locked" by the adaptor protein during substrate passage, possibly by interaction of its predicted α-helical regions (24) with the TolC tunnel helices. The operative details of export and efflux systems involving TolC remain to be established, but our results provide experimental support for a mechanism in which the crucial opening event is effected by realignment of the constrained inner coiled coils of the periplasmic tunnel.

This work was supported by grants from the Medical Research Council (to V.K. and C.H.) and the Biotechnology and Biological Sciences Research Council (to V.K.), and a European Molecular Biology Organization fellowship (to C.A.).

1. Thanassi, D. G. & Hultgren, S. J. (2000) *Curr. Opin. Cell. Biol.* **12,** 420–430.
2. Andersen, C., Hughes, C. & Koronakis, V. (2000) *EMBO Rep.* **1,** 313–318.
3. Thanabalu, T., Koronakis, E., Hughes, C. & Koronakis, V. (1998) *EMBO J.* **17,** 6487–6496.

4. Koronakis, V., Li, J., Koronakis, E. & Stauffer, K. (1997) *Mol. Microbiol.* **23,** 617–626.
5. Nikaido, H. (1994) *Science* **264,** 382–388.
6. Nikaido, H. (1998) *Curr. Opin. Microbiol.* **1,** 516–523.
7. Stone, B. J. & Miller, V. L. (1995) *Mol. Microbiol.* **17,** 701–712.
8. Bina, J. E. & Mekalanos, J. J. (2001) *Infect. Immun.* **69,** 4681–4685.
9. Koronakis, V., Sharff, A., Koronakis, E., Luisi, B. & Hughes, C. (2000) *Nature (London)* **405,** 914–919.
10. Koronakis, V., Andersen, C. & Hughes, C. (2001) *Curr. Opin. Struct. Biol.* **11,** 403–407.
11. Calladine, C. R., Sharff, A. & Luisi, B. (2001) *J. Mol. Biol.* **305,** 603–618.
12. Andersen, C., Hughes, C. & Koronakis, V. (2002) *J. Membr. Biol.* **185,** 83–92.
13. Benz, R., Maier, E. & Gentschev, I. (1993) *Zentralbl. Bakteriol.* **278,** 187–196.
14. Balakrishnan, L., Hughes, C. & Koronakis, V. (2001) *J. Mol. Biol.* **313,** 501–510.
15. Yanisch-Perron, C., Vieira, J. & Messing, J. (1985) *Gene* **33,** 103–119.
16. Koronakis, V., Koronakis, E. & Hughes, C. (1989) *EMBO J.* **8,** 595–605.
17. Andersen, C., Koronakis, E., Hughes, C. & Koronakis, V. (2002) *Mol. Microbiol.* **44,** 1131–1139.
18. Benz, R., Janko, K., Boos, W. & Lauger, P. (1978) *Biochim. Biophys. Acta* **511,** 305–319.
19. Sulavik, M. C., Houseweart, C., Cramer, C., Jiwani, N., Murgolo, N., Greene, J., DiDomenico, B., Shaw, K. J., Miller, G. H., Hare, R., *et al.* (2001) *Antimicrob. Agents Chemother.* **45,** 1126–1136.
20. Bayley, H. & Cremer, P. S. (2001) *Nature (London)* **413,** 226–230.
21. Chakraborty, T., Schmid, A., Notermans, S. & Benz, R. (1990) *Inf. Immun.* **58,** 2127–2132.
22. Song, L., Hobaugh, M. R., Shustak, C., Cheley, S., Bayley, H. & Gouaux, J. E. (1996) *Science* **274,** 1859–1866.
23. Gouaux, E. (1998) *J. Struct. Biol.* **121,** 110–122.
24. Johnson, J. & Church, G. M. (1999) *J. Mol. Biol.* **287,** 695–715.